Structure of Calmodulin Bound to a Calcineurin Peptide: A New Way of Making an Old Binding Mode † , ‡

ARTICLE *in* BIOCHEMISTRY · FEBRUARY 2006

Impact Factor: 3.02 · DOI: 10.1021/bi0521801 · Source: PubMed

5 AUTHORS, INCLUDING:

Qilu Ye
Queen's University
22 PUBLICATIONS **391** CITATIONS
SEE PROFILE

Qun Wei
Beijing Normal University
106 PUBLICATIONS **1,051** CITATIONS
SEE PROFILE

Structure of Calmodulin Bound to a Calcineurin Peptide: A New Way of Making an Old Binding Mode[†,‡]

Qilu Ye,[§,||,#] Xin Li,[§,#] Andrew Wong,[||] Qun Wei,*[,§] and Zongchao Jia*[,||]

Department of Biochemistry and Molecular Biology, Beijing Key Laboratory, Beijing Normal University, Beijing 100875, People's Republic of China, and Department of Biochemistry, Queen's University, Kingston, Ontario K7L 3N6, Canada

Received October 25, 2005; Revised Manuscript Received November 22, 2005

ABSTRACT: Calcineurin is a calmodulin-binding protein in brain and the only serine/threonine protein phosphatase under the control of Ca^{2+}/calmodulin (CaM), which plays a critical role in coupling Ca^{2+} signals to cellular responses. CaM up-regulates the phosphatase activity of calcineurin by binding to the CaM-binding domain (CBD) of calcineurin subunit A. Here, we report crystal structural studies of CaM bound to a CBD peptide. The chimeric protein containing CaM and the CBD peptide forms an intimate homodimer, in which CaM displays a native-like extended conformation and the CBD peptide shows α-helical structure. Unexpectedly, the N-terminal lobe from one CaM and the C-terminal lobe from the second molecule form a combined binding site to trap the peptide. Thus, the dimer provides two binding sites, each of which is reminiscent of the fully collapsed conformation of CaM commonly observed in complex with, for example, the myosin light chain kinase (MLCK) peptide. The interaction between the peptide and CaM is highly specific and similar to MLCK.

Calcineurin is the only known protein Ser/Thr phosphatase whose activity is regulated by calmodulin (*1*, *2*). Calcineurin is involved in many critical cellular processes, including T-cell activation, apoptosis, ion channel regulation, and cardiac myocyte hypertrophy (*3*−*6*). As a heterodimeric protein, calcineurin consists of a 61 kDa catalytic subunit A (CNA) and a 19 kDa regulatory subunit B (CNB). CNA contains four functional domains: a catalytic domain, a CNB binding domain, a calmodulin-binding domain (CBD), and an autoinhibitory domain (AID) (*7*−*10*). CNB has four EF-hands similar to those in calmodulin (*11*). Crystal structures of calcineurin have revealed that the catalytic domain is ellipsoidal and consists of a mixture of α-helices and *β*-sheets. The CNB binding domain protrudes from the ellipsoid, forming a five-turn α-helix connected to the catalytic domain via a short linker. The two globular domains of CNB are arranged linearly along the CNB binding domain and form a 33 Å long hydrophobic groove to associate with CNA (*8*, *9*). In total, there are four crystal structural studies of calcineurin and its various complexes, the first of which was reported almost a decade ago (*8*, *9*, *12*, *13*). However, the calmodulin-binding domain or CBD of calcineurin is notably absent from all published structures because this region is largely disordered in the absence of bound calmodulin. Therefore, the structure of the calmodulin-binding domain, its interaction with calmodulin, and activation of calcineurin by calmodulin remain unknown.

Calmodulin (CaM) is a ubiquitous and highly conserved acidic Ca^{2+}-binding protein, which regulates many cellular proteins and transmembrane ion transporters (*14*, *15*). The classic model of calmodulin binding to its target proteins or synthetic peptides involves the unwinding and bending of the central α-helix to bring the N- and C-terminal lobes in a collapsed conformation, thus, exposing hydrophobic grooves which interact with two hydrophobic anchor residues of a target molecule (*16*−*20*). But more recent structural studies have revealed that calmodulin can adopt a wide spectrum of conformations to interact with different targets. These include adopting an extended conformation (*21*−*23*), absence of the hydrophobic pocket in the N-terminal lobe (*24*), formation of a different loop from the central linker for peptide interaction (*25*), binding of Ca^{2+} ions in only one EF-hand pair (*22*, *23*), binding to the target peptide only with the C-terminal lobe (*21*), binding to the myristoyl moiety of the target peptide (*26*), and promoting target dimer formation (*22*). These results clearly demonstrate the diversity of conformations that calmodulin is able to adopt in accommodating different binding partners.

In this study, we have generated a fusion protein in which a 25-residue peptide (residues 389−413, sequence AAARKEVIRNKIRAIGKMARVFSVL) derived from CBD of calcineurin subunit A was fused to the C-terminus of calmodulin via a 5-glycine flexible linker (Figure 1). The crystal structure of this fusion protein, which we shall refer to as CcL (Calmodulin fused to calmodulin-binding domain of calcineurin via a Linker), is reported here.

[†] This work was supported in part by grants from the National Natural Science Foundation of China, the Research Fund for the Doctoral Program of High Education, the National Important Basic Research Project, and Canadian Institutes of Health Research.

* Conresponding authors. For Z.J.: phone, 1 613 533 6277; fax, 1 613 533 2497; e-mail, jia@post.queensu.ca. For Q.W.: e-mail, weiq@bnu.edu.cn.

[‡] The coordinates for CcL in two different crystal forms (space groups *P*321 and *C*2) have been deposited in the Protein Data Bank as entries 2F2P and 2F2O for *P*321 and *C*2, respectively.

[§] Beijing Normal University.

[||] Queen's University.

[#] These authors contributed equally.

10.1021/bi0521801 CCC: $33.50
Published on Web 12/22/2005

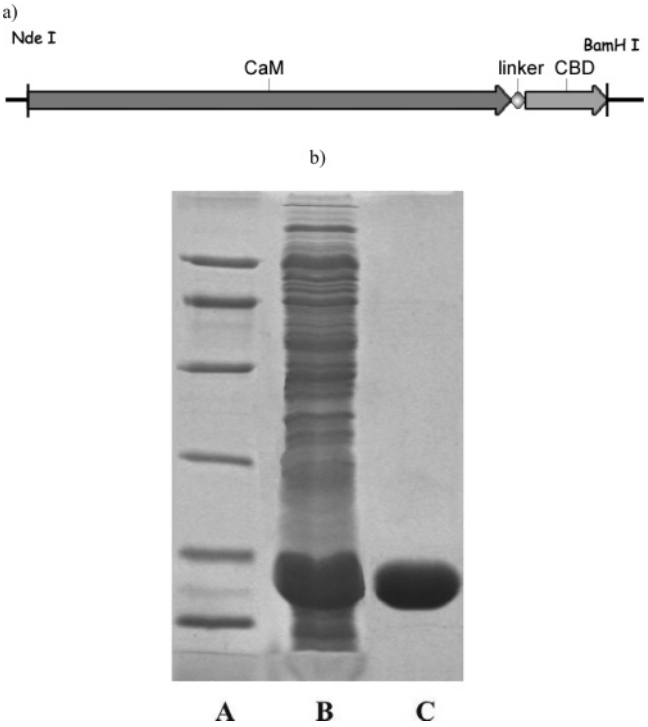

FIGURE 1: CcL construct and SDS gel of its expression and purification. (a) The C-terminus of CaM is fused to the N-terminus of the CBD peptide through a 5-glycine linker. (b) Lane A, molecular weight standard; lane B, supernatant of lysate; lane C, purified CcL.

MATERIALS AND METHODS

Materials. IPTG, Tris, EDTA, $MnCl_2$, and $CaCl_2$ were purchased from Sigma (St. Louis, MO). Restriction enzymes (Nde I and Bam HI), T4 DNA ligase, and Pyrobest polymerase were purchased from TaKaRa Biotech (Tokyo, Japan). Protein standard was obtained from Sigma and DEAE Sepharose FF from Amersham Biosciences (Uppsala, Sweden). All other reagents used were of analytical grade.

Construction of Expression Vector pETCcL. A three-step PCR procedure was employed to create the fusion protein CcL. The primers and PCR strategies used are described below. Sequences complementary to templates are underlined, STOP codon is in italics, and glycine codons are in bold type. In the first PCR reaction, the sense primer (carrying Nde I site), 5′-CCGCCATATGGCTGATCAACTGACA-3′, and the antisense primer, 5′-TGCAGC**ACCACCACCGCCACC**CTTCGCTGTCATCATCTG-3′, were used with the plasmid pETCaM (*27*) as template. In the second PCR reaction, the sense primer, 5′-GCGAAG**GGTGGCGGTGGTGGT**GCTGCAGCCCGGAAGGAG-3′, and antisense primer (carrying Bam HI site), 5′-CGCGGGATCC*TTA*GAGAACTGAGAATACTCT-3′, were used with the plasmid pETCNA vector (*28*) as template. The two PCR products were partly complementary to each other and were used as templates in the third PCR reaction together with the primary sense and the secondary antisense primers. The final PCR product and the blank pET21a plasmid were cut with Nde I and Bam HI. Positive recombinant colonies were obtained after standard ligation, transformation, and plasmid screening, and the complete sequence of CcL was confirmed by DNA sequencing.

Expression and Purification of CcL. A single colony of *Escherichia coli* strain BL21 (DE3)/pETCcL from a freshly streaked plate was inoculated into 50 mL of LB media containing 100 μg/mL ampicillin and incubated with shaking at 37 °C overnight; the growth was used to inoculate 2 L of TM containing 100 μg/mL ampicillin. When OD_{600} reached 1.0, IPTG was added to 0.5 μM, and the culture was shaken continuously at 28 °C for another 16 h. The cells were harvested by centrifugation at 10 000*g* for 10 min.

The cell pellet was washed once with 100 mL of lysis buffer (50 mM Tris-HCl, pH 7.4, and 1 mM EDTA), then completely resuspended in 200 mL of lysis buffer with 0.2 mM phenylmethylsulfonyl fluoride (PMSF) and 20 mM β-mercaptoethanol, and the cells were lysed by sonication. The lysate was clarified by centrifugation at 40 000*g* for 20 min. The supernatant was transferred to a flask, which was placed in an 85 °C water bath and kept for 20 min. The precipitate was removed by centrifugation at 40 000*g* for 20 min. The supernatant was diluted 2-fold with Milli-Q water and adjusted to pH 7.4 with 1 M Tris base. The sample was applied to a DEAE column preequilibrated with 20 mM Tris-HCl, pH 7.4, and mounted to a fast protein liquid chromatography (FPLC) system (Amersham). The column was washed with the same buffer and eluted with 20 mM Tris-HCl, pH 7.4, and 100 mM NaCl. Fractions of 2.5 mL were collected, and the purity of the protein was analyzed by 12% SDS−PAGE.

To assess oligomeric state of CcL in solution, we performed gel filtration experiements. At protein concentration of 2 mg/mL, 0.5 mL CcL was loaded onto a Superdex 75 column (column volume: 120 mL). The running buffer was 20 mM Tris-HCl (pH 7.4), and 1 mM $CaCl_2$. The Superdex 75 column was fully calibrated.

Assay of Phosphatase Activity. The phosphatase activity of CNA was assayed in the *p*-nitrophenyl (pNPP) substrate solution containing 50 mM Tris-HCl, pH 7.4, 0.5 mM $MnCl_2$, 1 mM $CaCl_2$, 0.5 mM DTT, 0.2 mg/mL bovine serum albumin, and 20 mM *p*-nitrophenyl phosphate. CNB was added to the substrate solution to a final concentration of 2 μM when using CNB to stimulate CNA phosphatase activity. Measurements using CaM or CcL to stimulate CNA phosphatase activity used a ratio of CaM or CcL to CNA of 2:1 on a molar basis. The reactions were performed in a 0.2 mL volume at 30 °C for 20 min and terminated by the addition of 1.8 mL of a 0.5 mM Na_2CO_3 and 20 mM EDTA solution. The absorbance was measured at 410 nm. The units (U) of activity are defined as nanomole of pNPP hydrolyzed per minute.

Crystallization and Data Collection. CcL was crystallized at room temperature by hanging-drop vapor-diffusion method, in the presence of 1 mM calcium. Two different crystal forms, hexagonal and plate-shaped, were obtained. Hexagonal crystals were grown from 29% PEG monomethyl ether 2K, 0.2 M ammonium sulfate, and 0.1 M malonic acid, pH 4.5. Plate crystals were obtained from a different buffer (0.1 M citrate, pH 4.5).

X-ray diffraction data were collected at NSLS. The hexagonal crystal diffracted to 2.6 Å in space group *P*321, with cell parameters $a = b = 137.7$ Å, $c = 45.3$ Å. The plate crystal diffracted to 2.17 Å in space group *C*2, with cell parameters $a = 116.2$ Å, $b = 41.9$ Å, $c = 69.6$ Å, $\beta = 110.5°$. Both crystal forms have two molecules in the asymmetric unit. Each data set was collected from a single-crystal cryo-cooled to 100 K. The data were processed and

Table 1: Diffraction and Structure Refinement Statistics

Crystal Parameters and Data Statistics		
space group	*C*2	*P*321
cell dimension (Å)		
a	116.19	137.72
b	41.85	137.72
c	69.64	45.28
solvent content (%)	39	60
no. of molecules in ASU	2	2
resolution range (Å)	50−2.17	50−2.60
total no. of reflections	346901	256617
no. of unique reflections	18125	15794
R_{sym}	0.057	0.096
completeness (%)	97.6	99.5
Refinement Statistics		
resolution range (Å)	50−2.17	50−2.60
sigma cutoff for refinement	none	none
R (R_{free})	20.4% (28.9%)	23.4% (29.7%)
no. of reflections in test set (%)	1774 (9.9%)	1495 (9.4%)
no. of non-hydrogen protein atoms	2494	2666
no. of calcium atoms	8	8
no. of water molecules	178	32
rmsd bond lengths (Å)	0.003	0.011
rmsd bond angles (deg)	1.34	1.29

scaled with DENZO and SCALEPACK (*29*). The statistics of the diffraction data are summarized in Table 1.

Structure Determination and Refinement. The structure was solved by molecular replacement (MR) using a previously solved calmodulin complex structure devoid of the peptide from the CaM-binding domain of CaM-dependent protein kinase II (PDB accession code: 1CDM) as a search model. For MR calculations, the program PHASER was used (*30*). An initial attempt to use the entire collapsed CaM molecule (1CDM) as the search model was unsuccessful. It is well-known that the central helical region of CaM can be very flexible; therefore, further MR was carried out using the two individual halves of CaM. Using the N-terminal lobe (residues 4−73) of CaM as a search model, we obtained two solutions with least-likelihood gain (LLG) of 107 and a *Z*-score of 10.97 from PHASER (*30*). By fixing the two N-terminal lobes, we identified two additional solutions with LLG of 398 and a *Z*-score of 13.45 using the C-terminal (residues 84−116) lobe as a search model. After several rounds of CNS (*31*) refinement and manual model editing with XFIT (*32*), the central helical region of CaM as well as the fused peptide could be clearly seen at 3σ levels of the $F_o - F_c$ difference density map. However, the initial assignment of the N- and C-terminal lobes from the MR solutions was found to be incorrect. On the basis of the connections of the central helical region, one of the initial N-terminal lobes was actually a C-terminal lobe, and vice versa. $F_o - F_c$ difference densities of at least 4σ levels were also found in each of the eight EF-hand motifs, corresponding to bound calcium ions. CNS (*31*) was used for the addition of water molecules to the models. The model in the *C*2 space group was further refined by REFMAC (*33*) with each CaM molecule and peptide sequence defined as individual TLS (*34*) groups.

RESULTS AND DISCUSSION

Preparation of CcL and Its Activation on CNA. CcL was highly expressed as a soluble cytosolic protein in *E. coli.* More than 100 mg of purified protein were obtained from 1 L of cell culture (Figure 1). CaM induces a 2-fold increase in the phosphatase activity of CNA in the absence or presence of CNB, as evident in Figure 2. As expected, in contrast, CcL has no effect on the activity of CNA, evidently suggesting that the CBD peptide has taken up the binding position in CaM and prevented CaM from binding the target molecule CNA.

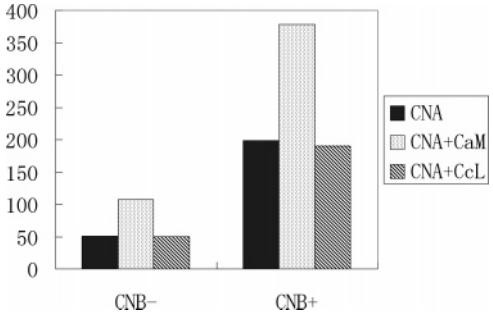

FIGURE 2: Activation of CNA by CaM and CcL. When pNPP was used as a standard substrate, the phosphatase activity of isolated CNA was 51.2 units/mg. Upon addition of CaM or CcL, the phosphatase activity of CNA was 107.5 units/mg or 50.2 units/mg, respectively. In the presence of CNB, the phosphatase activity of CNA was 199.2 units/mg. When mixed with CaM or CcL, the activity of CNA in the presence of CNB was 378.0 units/mg or 190.2 units/mg, respectively.

As demonstrated by gel filtration (Figure 3), more than 10% of CcL existed as dimer. The characteristic monomer, as expected from our experience, was the dominant peak. To ascertain the identity of the small peak, an SDS−PAGE gel was run, and the result confirmed it was CcL. We have further carried out analytical ultracentrification experiments (protein concentration of 2 mg/mL in 20 mM Tris-HCl, pH 7.4, and 1 mM $CaCl_2$). The result also indicated the existence of a small amount of CcL dimer (data not shown).

Overall Structure. We have determined the crystal structures of CcL in two different crystal forms (space group *C*2 and *P*321) in the presence of Ca^{2+}. The final R/R_{free} factors are 0.234/0.297 for the *P*321 structure at 2.6 Å resolution and 0.204/0.289 for the *C*2 structure at 2.17 Å resolution, respectively (Table 1). Since the *P*321 data is of lower resolution, the slightly higher *R*-factors are not surprising. For the *C*2 crystal, the diffraction was somewhat isotropic, as in certain regions the diffraction was much worse than others. This may have contributed to the relatively high R_{free} value. The coordinates have been deposted (PDB accession codes: 2F2P for *P*321 and 2F2O for *C*2). The final structures from the two crystal forms are nearly identical, with root-mean-square deviation (rmsd) of only 0.94 Å. Not surprisingly, the individual N- and C-lobes between the two crystal forms overlap slightly better (average rmsd of 0.85 Å). In both crystal forms, CcL forms a tight dimer, in which two CaM molecules associate in a head-to-tail manner (Figure 4). The two monomers are essentially identical, displaying an rmsd of 0.63 Å for the *C*2 structure and 0.50 Å for the *P*321 structure, respectively. As illustrated in Figure 4, the two CaM molecules maintain an extended conformation, similar to the open structure of the native Ca^{2+}/CaM in the absence of ligand (*35*, *36*) with an rmsd of 1.7 Å. As expected, eight Ca^{2+} ions are bound in the four EF-hand lobes in two CaM molecules. The two CBD peptides are bound at equivalent positions between the N-terminal lobe of the first CaM molecule and the C-terminal lobe of the

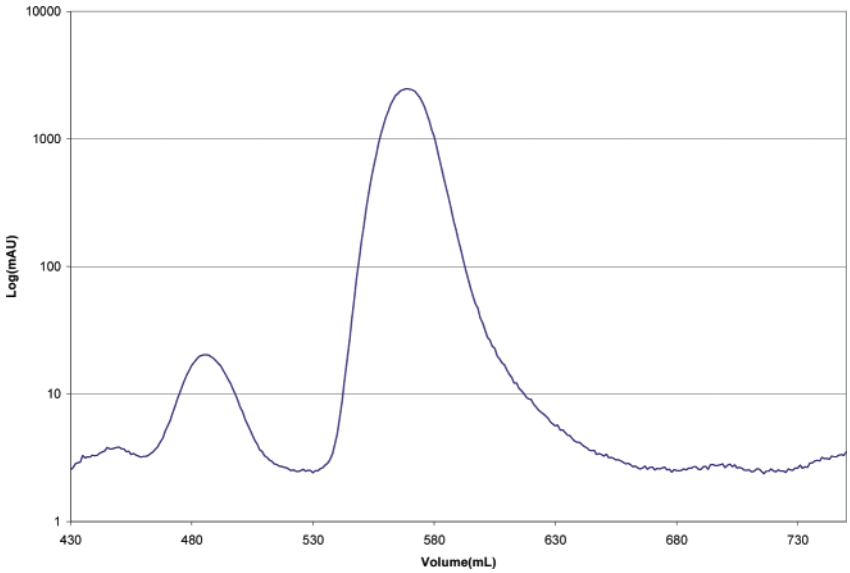

FIGURE 3: Gel filtration of CcL. The major peak is CcL monomer, while the smaller peak corresponds to the dimer.

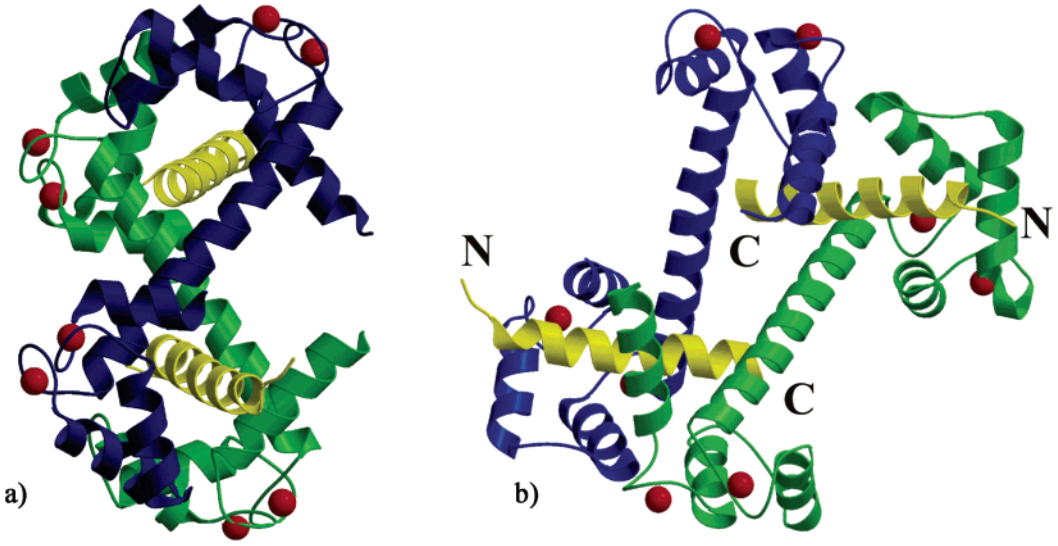

FIGURE 4: Overall dimer structure of CcL. (a) The top half represents N1 (blue) and C2 (green) assembly, with the peptide (yellow) trapped between N1 and C2. Ca^{2+} ions are shown in red spheres. There is a pseudo two-fold rotation symmetry running horizontally through the center of the dimer. (b) Side view of the CaM dimer, rotated approximately 90° around the central vertical axis from panel a. The two peptides run in opposite direction. The N- and C-termini of the peptides are highlighted. Minimally ~9 amino acids would be required to link N- and C-termini of the peptide.

second CaM molecule. A single CaM moiety in the CcL dimer exhibits the classical extended conformation and dumbbell-folding topology with maximum length of ~63 Å. It is very similar to the structure of the ligand-free CaM structure (*35*, *36*) which has maximum length of ~65 Å. The rmsd between the two structures is only 1.7 Å for all Cα atoms. As in the ligand-free Ca^{2+}/CaM structure, the central helix between the N- and C-lobes of CaM monomer is fully retained, showing no sign of bending and/or unwinding (Figure 5). Interestingly, only a few direct contacts are observed between two CaM monomers (Ser38A−Lys94B, Ser38A−Asn111B, Asn111A−Lys21B). Instead, the dimer formation is mainly mediated by the bound CBD peptides (see below).

Novel Binding Conformation. In the CcL structure, the two extended CaM molecules form an "X-shaped" dimer, in which each of the "V-shaped" halves at the top and bottom houses one CBD peptide-binding site. Each novel CBD-binding site is composed of the N-lobe of one CaM molecule and the C-lobe of the other CaM molecule, conveniently described as N1−C2. Most interestingly, this N1−C2 configuration assumes an ellipsoidal shape of approximately 50 × 29 × 25 Å that closely resembles the collapsed conformation of the ligand-bound CaM, such as CaM in complex with the smooth muscle myosin light chain kinase (smMLCK) peptide (*19*). The CaM−smMLCK complex shows that the α-helix of the central linker of CaM is unwound to allow the N- and C-lobes to bend by ~100° and rotate by ~120°, forming a collapsed and compact conformation (*19*, *20*) which has dimensions of 50 × 30 × 25 Å (*18*). The rmsd between the N1−C2 assembly and the CaM−smMLCK structure is 1.9 Å for Cα atoms (Figure 6). The subtle difference between the two structures is the relative position of the N- and C-lobes, which differ by ~10°.

The N- and C-lobes in N1−C2 are associated with a number of contacts involving several hydrophobic residues

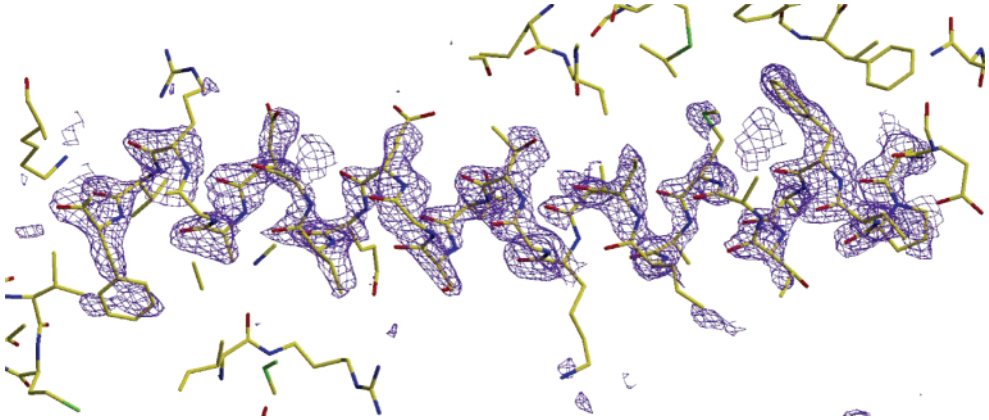

FIGURE 5: Omit $F_o - F_c$ electron density map of the central α-helix of one CaM molecule. In total, 29 residues of the central α-helical linker (bovine CaM sequence 65−93) were omitted in the refinement and the subsequent map calculation. For the purpose of comparison, the 29 residues in the final structure are shown together with the map. The map is contoured at 2.5σ.

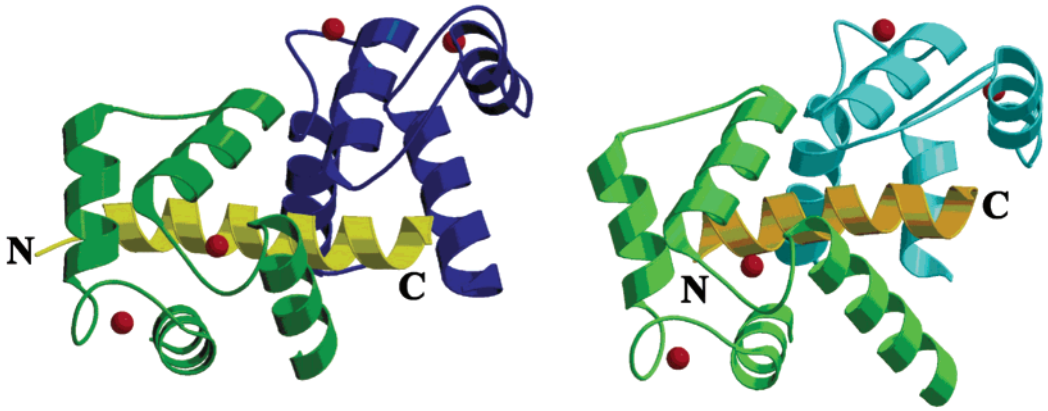

FIGURE 6: Comparison between the CcL N1−C2 assembly with the peptide bound (left) and the CaM−smMLCK complex (right). Peptides are shown in yellow/brown; N-lobe and C-lobe are shown in green and blue, respectively. The N- and C-termini of the peptides are highlighted.

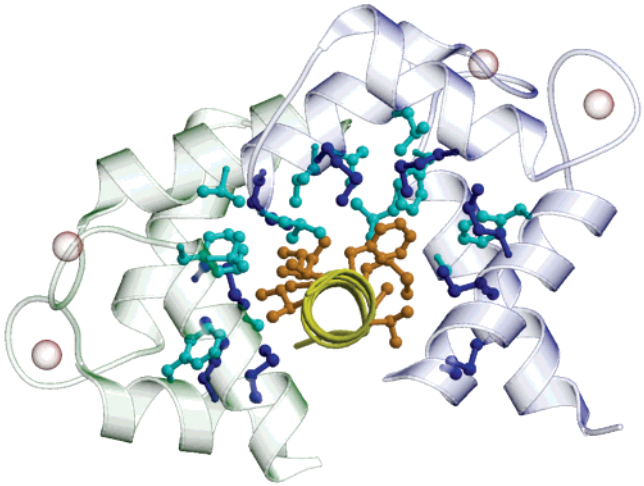

FIGURE 7: Close view to show detailed interaction between the CBD peptide and N1−C2. All hydrophobic residues involved in the interaction are shown. CaM is shown in transparent and the peptide backbone in yellow. Side chains of hydrophobic residues of the peptide are highlighted in orange. Met residues of CaM are displayed in blue, and the rest of hydrophobic residues are in cyan.

in helix II in N1 and helix VI in C2 such as Leu32, Thr34, Val35, Met36, Ser38, and Leu39 in helix II from N1 and Leu105, Val108, Met109, Thr110, and Leu112 in helix VI from C2 (Figure 7). These residues are exposed to the solvent and form a large hydrophobic channel on the surface, similar to other collapsed CaM−ligand complexes such as CaM−smMLCK. Although the distribution of hydrophobic residues, spatial organization of the EF-hands, conformation of EF-hands between CcL, and the CaM−smMLCK structure are all very similar, it has not been shown before that CaM is able to accomplish this via formation of a "heterodimer" involving intermolecular N- and C-lobes. Furthermore, the extended conformation of each CaM in the N1−C2 configuration does not bear resemblance to the CaM/K^+ channel complex, in which the CaM moieties also retain an extended conformation. In the CaM/K^+ channel complex, two extended CaM molecules mediate the dimerization of the target protein, while the N-lobe and C-lobe of each CaM molecule make contacts with different regions of the CaM-binding domain of the K^+ channel (*22*). In contrast, the CaM molecules in the CcL dimer bind two α-helical peptides in an identical fashion (Figure 4a). Taken together, our observations suggest that the N1−C2 assembly represents yet another novel conformation of CaM.

Interaction of the CBD Peptide. Of the 25 residues of the calmodulin-binding domain (CBD) peptide, 23 residues (residues 389−411 in CNA numbering) were observed with clear electron density, all of which are in contacts with N1−C2 (<4 Å). The two remaining C-terminal residues of the CBD peptide and the glycine linker were not visible, a significant observation clearly indicating that the linker remains completely disordered and mobile. The peptide folds into an amphiphilic α-helix and is embraced by N1 and C2 (Figure 4a). The conserved hydrophobic residues Ile396,

Ile400, Ile403, and Val 409 in the CcL peptide form a 1-5-8-14 hydrophobic motif (*37*), which points to one side of the hydrophobic concave patch between N1 and C2. Met406, Ala407, and Phe410 are also in close proximity to the hydrophobic surface cavities and are involved in the hydrophobic interaction with CaM (Figure 7). The positions of these three hydrophobic residues in the CcL structure are similar to their counterparts, Ala809, Ile810 and Leu813, in the CaM−smMLCK complex (*19*). The orientation of the CBD peptide is also identical to the kinase peptide in CaM−smMLCK, with its N-terminus pointing to the C2. As expected, all of the Met residues of N1−C2 except Met76 are involved in interaction with the peptide, again akin to CaM−smMLCK. Despite the high similarity, there are several small differences. The hydrophobic anchor residues in the CBD peptide are farther apart, separated by 13 residues (Ile396 and Phe410), rather than the 12 residues (Trp800 and Leu813) in CaM−smMLCK. Ala402 in the CBD peptide points to the helix I hydrophobic residue cluster (particularly Ala15) in N1. Gly404 of the peptide is close to Ala88 in C2. Interestingly, their counterparts His805 and Arg808 in smMLCK are hydrophilic residues. There are a total of nine (Ile396, Ile400, Ala402, Ile403, Gly404, Met406, Ala407, Val409, and Phe410) hydrophobic anchor residues in the CBD peptide to participate in hydrophobic interaction with N1−C2, rather than seven in CaM−smMLCK. Arg812 in the peptide of CaM−smMLCK is the only residue that forms a hydrogen bond and salt bridge with CaM; this helps maintain the bent structure (*19*). However, in the CBD peptide, two additional residues Arg401 and Phe410 form hydrogen bonds with N1−C2. Furthermore, Arg408 (Arg812 in CaM−smMLCK) in the CBD peptide forms salt bridges with Glu83 of N1. The increased interactions seen in CcL not only enhance the association between the CBD peptide and CaM but also play a key role to facilitate and sustain the compact N1−C2 conformation of CaM.

In the CcL structure, N1 and C2 of CaM recognize and bind CBD peptide without any involvement of the central helices. The helical structure of the central linker is fully retained (Figure 7). The peptide makes no direct interaction with either the N-terminal half of the helix from the first CaM molecule or the C-terminal half of the helix from the second CaM molecule. This observation is in agreement with the previous report (*38*) that showed mutations of the central helix have minimal effect on the function of CaM. In other CaM−peptide complexes such as CaM−smMLCK complex (*19*), no direct contacts exist between the peptide and the central α-helix. Our results support the notion that the function of the central helix is simply to afford CaM the flexibility to allow the two lobes to move to their appropriate positions for interaction with target molecules.

Implication of the Novel Dimer Conformation. In this particular case where calcineurin is the substrate of CaM, obviously the N1−C2 conformation of CaM cannot be physiologically relevant as there is only one CaM-binding site in calcineurin. Additionally, it has been demonstrated that calcineurin and CaM form a binary complex instead of a tetramer (*1*), which would be formed through CcL-like interaction. However, it is important to stress that this "artifical" CcL construct is indeed able to form dimers in solution (Figure 3). Indeed, native CaM can also form a dimer as shown by several biophysical techniques including ultrahigh-resolution electrospray ionization mass spectra (*39*), although biological implication of such a native CaM dimer is not clear. Dimer formation is one of the many recognition strategies used by CaM. CaM recognizes and binds to the IQ motif ([I,L,V]QXXXRXXXX[R,K]) found in many proteins, some of which contain multiple IQ motifs to regulate a wide diversity of biological functions (*40*). In some proteins that act in a Ca^{2+}-dependent manner, the IQ motif may either conform to a 1-5-8-14 motif (*37*), which is similar to the CBD peptide, or act to bind and retain CaM at low Ca^{2+} levels. In myosins and some nonmyosin proteins, there are multiple 14-residue motifs that are separated by 9−16 residues (*40*). We envisage that the novel CaM dimerization strategy is especially useful for targeting proteins that contain multiple IQ motifs. If such a speculation is validated, the CaM dimer structure would be able to bind two IQ sites simultaneously. We estimate that at least ∼9 residues are necessary to connect the N- and C-termini of the two peptides in the CcL dimer structure (Figure 4b), in excellent agreement with the minimum separation between IQ motifs. As an analogy, the dimer structure is similar to a linkage of two levers with the fulcrum in the center of the two CaM α-helical linkers. The four arms of the levers, which are the N-lobes and C-lobes of two CaM molecules, hold the target peptides in place. Additionally, the novel dimerization strategy could also serve as another mechanism by which CaM mediates the dimerization of the target proteins as in the case of CaM in complex with CaM-binding domain of K^+ channel (*22*), where it forms an elongated dimer with two CaM molecules bound at both ends. Each CaM wraps around three α-helices, two from one subunit of CaM-binding domain of the K^+ channel and one from the other.

It is becoming clear that CaM is able to adopt a multitude of conformations in order to interact specifically with a plethora of target proteins. Such conformational plasticity appears to rely on the flexibility of its central α-helical linker, which allows juxtaposition of the N- and C-lobes in the appropriate configurations for optimal contacts with the target proteins.

To circumvent difficulties in obtaining cocrystals of the CaM−calcineurin or CaM−CBD peptide complexes, we have succeeded in solving the structure of a fusion protein consisting of CaM covalenly linked to a CBD peptide. One potential caveat of this approach is that the structure of the fusion protein may deviate from that of the natural complex due to constraint in the movement of the peptide and CaM. It is important to note that, in the complex structure of CaM−smMLCK, the closest Cα distance between the N-terminal region of the peptide and the C-terminal end of CaM is <9 Å. Such a short distance would be readily covered by only three residues. Thus, the 5-Gly linker, which is flexible and long enough, would reduce the constrains on the CBD peptide in intereacting with CaM. In fact, invisibility of all five glycine residues in the electron density map provides direct evidence to support the notion that the linker remains completely free and mobile as previously alluded. We therefore conclude that the novel CaM conformation is unlikely an "artifact" of the fusion protein.

Structural data of the CcL complex reported here will provide insights into CaM interaction with target proteins containing multiple CaM-binding sites such as IQ motifs. This work once again exemplifies the diversity of CaM

binding conformation and its resulting versatile ability to recognize and regulate a wide variety of target molecules. This novel finding adds to the ever increasing diversity of CaM binding conformations, and we expect more CaM conformations to be discovered.

ACKNOWLEDGMENT

Access to beamline X8C at Brookhaven National Laboratory is greatly appreciated. We thank Drs. G. Cote, A. Mak, and J. Elce for critical discussion. We are also grateful to the Protein Function Discovery facility at Queen's University for helping perform the analytical ultracentrification experiments. Z.J. is the recipient of an NSERC Steacie Fellowship and a Canada Research Chair for Structural Biology.

REFERENCES

1. Klee, C. B., Crouch, T. H., and Krinks, M. H. (1979) Calcineurin: a calcium- and calmodulin-binding protein of the nervous system, *Proc. Natl. Acad. Sci. U.S.A. 76*, 6270−6273.
2. Klee, C. B., Draetta, G. F., and Hubbard, M. J. (1988) Calcineurin, *Adv. Enzymol. Relat. Areas Mol. Biol. 61*, 149−200.
3. Clipstone, N. A., and Crabtree, G. R. (1993) Calcineurin is a key signaling enzyme in T lymphocyte activation and the target of the immunosuppressive drugs cyclosporin A and FK506, *Ann. N. Y. Acad. Sci. 696*, 20−30.
4. Iwata, M., Ohoka, Y., Kuwata, T., and Asada, A. (1996) Regulation of T cell apoptosis via T cell receptors and steroid receptors, *Stem Cells 14*, 632−641.
5. Swope, S. L., Moss, S. J., Raymond, L. A., and Huganir, R. L. (1999) Regulation of ligand-gated ion channels by protein phosphorylation, *Adv. Second Messenger Phosphoprotein Res. 33*, 49−78.
6. Molkentin, J. D., Lu, J. R., Antos, C. L., Markham, B., Richardson, J., Robbins, J., Grant, S. R., and Olson, E. N. (1998) A calcineurin-dependent transcriptional pathway for cardiac hypertrophy, *Cell 93*, 215−228.
7. Hubbard, M. J., and Klee, C. B. (1989) Functional domain structure of calcineurin A: mapping by limited proteolysis, *Biochemistry 28*, 1868−1874.
8. Hashimoto, Y., Perrino, B. A., and Soderling, T. R. (1990) Identification of an autoinhibitory domain in calcineurin, *J. Biol. Chem. 265*, 1924−1927.
9. Griffith, J. P., Kim, J. L., Kim, E. E., Sintchak, M. D., Thomson, J. A., Fitzgibbon, M. J., Fleming, M. A., Caron, P. R., Hsiao, K., and Navia, M. A. (1995) X-ray structure of calcineurin inhibited by the immunophilin−immunosuppressant FKBP12−FK506 complex, *Cell 82*, 507−522.
10. Kissinger, C. R., Parge, H. E., Knighton, D. R., Lewis, C. T., Pelletier, L. A., Tempczyk, A., Kalish, V. J., Tucker, K. D., Showalter, R. E., and Moomaw, E. W. (1995) Crystal structures of human calcineurin and the human FKBP12−FK506−calcineurin complex, *Nature 378*, 641−644.
11. Aitken, A., Klee, C. B., and Cohen, P. (1984) The structure of the B subunit of calcineurin, *Eur. J. Biochem. 139*, 663−671.
12. Huai, Q., Kim, H. Y., Liu, Y., Zhao, Y., Mondragon, A., Liu, J. O., and Ke, H. (2002) Crystal structure of calcineurin−cyclophilin−cyclosporin shows common but distinct recognition of immunophilin−drug complexes, *Proc. Natl. Acad. Sci. U.S.A. 99*, 12037−12042.
13. Jin, L., and Harrison, S. C. (2002) Crystal structure of human calcineurin complexed with cyclosporin A and human cyclophilin, *Proc. Natl. Acad. Sci. U.S.A. 99*, 13522−13526.
14. Cohen, P., and Klee, C. B. (2005) *Calmodulin*, Elsevier, Amsterdan.
15. Eldik, L. V., and Watterson, D. (2005) *Calmodulin and Signal Transduction*, Academic Press, New York.
16. O'Neil, K. T., and DeGrado, W. F. (1989) The interaction of calmodulin with fluorescent and photoreactive model peptides: evidence for a short interdomain separation, *Proteins 6*, 284−293.
17. Vorherr, T., Kessler, O., Mark, A., and Carafoli, E. (1992) Construction and molecular dynamics simulation of calmodulin in the extended and in a bent conformation, *Eur. J. Biochem. 204*, 931−937.
18. Ikura, M., Clore, G. M., Gronenborn, A. M., Zhu, G., Klee, C. B., and Bax, A. (1992) Solution structure of a calmodulin−target peptide complex by multidimensional NMR, *Science 256*, 632−638.
19. Meador, W. E., Means, A. R., and Quiocho, F. A. (1992) Target enzyme recognition by calmodulin: 2.4 Å structure of a calmodulin−peptide complex, *Science 257*, 1251−1255.
20. Meador, W. E., Means, A. R., and Quiocho, F. A. (1993) Modulation of calmodulin plasticity in molecular recognition on the basis of X-ray structures, *Science 262*, 1718−1721.
21. Elshorst, B., Hennig, M., Forsterling, H., Diener, A., Maurer, M., Schulte, P., Schwalbe, H., Griesinger, C., Krebs, J., Schmid, H., Vorherr, T., and Carafoli, E. (1999) NMR solution structure of a complex of calmodulin with a binding peptide of the Ca^{2+} pump, *Biochemistry 38*, 12320−12332.
22. Schumacher, M. A., Rivard, A. F., Bachinger, H. P., and Adelman, J. P. (2001) Structure of the gating domain of a Ca^{2+}-activated K^+ channel complexed with Ca^{2+}/calmodulin, *Nature 410*, 1120−1124.
23. Drum, C. L., Yan, S. Z., Bard, J., Shen, Y. Q., Lu, D., Soelaiman, S., Grabarek, Z., Bohm, A., and Tang, W. J. (2002) Structural basis for the activation of anthrax adenylyl cyclase exotoxin by calmodulin, *Nature 415*, 396−402.
24. Yamauchi, E., Nakatsu, T., Matsubara, M., Kato, H., and Taniguchi, H. (2003) Crystal structure of a MARCKS peptide containing the calmodulin-binding domain in complex with Ca^{2+}-calmodulin, *Nat. Struct. Biol. 10*, 226−231.
25. Aoyagi, M., Arvai, A. S., Tainer, J. A., and Getzoff, E. D. (2003) Structural basis for endothelial nitric oxide synthase binding to calmodulin, *EMBO J. 22*, 766−775.
26. Matsubara, M., Nakatsu, T., Kato, H., and Taniguchi, H. (2004) Crystal structure of a myristoylated CAP-23/NAP-22 N-terminal domain complexed with Ca(2+)/calmodulin, *EMBO J. 23*, 712−718.
27. Qin, Y., Liu, J., Li, X., and Wei, Q. (2005) Preparation and characterization of a single-chain calcineurin−calmodulin complex, *Biochim. Biophys. Acta 1747*, 171−178.
28. Wei, Q., and Lee, E. Y. (1997) Expression and reconstitution of calcineurin A and B subunits, *Biochem. Mol. Biol. Int. 41*, 169−177.
29. Otwinowski, Z., and Minor, W. (1997) Processing of X-ray diffraction data collected in oscillation mode, *Methods Enzymol. 276*, 307−326.
30. Storoni, L. C., McCoy, A. J., and Read, R. J. (2004) Likelihood-enhanced fast rotation functions, *Acta Crystallogr., Sect. D: Biol. Crystallogr. 60*, 432−438.
31. Brunger, A. T., Adams, P. D., Clore, G. M., DeLano, W. L., Gros, P., Grosse-Kunstleve, R. W., Jiang, J. S., Kuszewski, J., Nilges, M., Pannu, N. S., Read, R. J., Rice, L. M., Simonson, T., and Warren, G. L. (1998) Crystallography & NMR system: a new software suite for macromolecular structure determination, *Acta Crystallogr., Sect. D: Biol. Crystallogr. 54* (Pt 5), 905−921.
32. McRee, D. E. (1999) XtalView/Xfit− A versatile program for manipulating atomic coordinates and electron density, *J. Struct. Biol. 125*, 156−165.
33. Murshudov, G. N., Vagin, A. A., Lebedev, A., Wilson, K. S., and Dodson, E. J. (1999) Efficient anisotropic refinement of macromolecular structures using FFT, *Acta Crystallogr., Sect. D: Biol. Crystallogr. 55* (Pt 1), 247−255.
34. Winn, M. D., Isupov, M. N., and Murshudov, G. N. (2001) Use of TLS parameters to model anisotropic displacements in macromolecular refinement, *Acta Crystallogr., Sect. D: Biol. Crystallogr. 57*, 122−133.
35. Chattopadhyaya, R., Meador, W. E., Means, A. R., and Quiocho, F. A. (1992) Calmodulin structure refined at 1.7 Å resolution, *J. Mol. Biol. 228*, 1177−1192.
36. Kuboniwa, H., Tjandra, N., Grzesiek, S., Ren, H., Klee, C. B., and Bax, A. (1995) Solution structure of calcium-free calmodulin, *Nat. Struct. Biol. 2*, 768−776.
37. Rhoads, A. R., and Friedberg, F. (1997) Sequence motifs for calmodulin recognition, *FASEB J. 11*, 331−340.
38. Tabernero, L., Taylor, D. A., Chandross, R. J., VanBerkum, M. F., Means, A. R., Quiocho, F. A., and Sack, J. S. (1997) The structure of a calmodulin mutant with a deletion in the central

helix: implications for molecular recognition and protein binding, *Structure 5*, 613−622.
39. Lafitte, D., Heck, A. J., Hill, T. J., Jumel, K., Harding, S. E., and Derrick, P. J. (1999) Evidence of noncovalent dimerization of calmodulin, *Eur. J. Biochem. 261*, 337−344.
40. Bahler, M., and Rhoads, A. (2002) Calmodulin signaling via the IQ motif, *FEBS Lett. 513*, 107−113.

BI0521801